

Fabrication of optical waveguides in RbTiOPO₄ single crystals by using different techniques

M. A. Butt^{a,b}, M. C. Pujol^a, R. Solé^a, A. Ródenas^a, G. Lifante^c, M. Aguiló^a, F. Díaz^a, S. N. Khonina^{b,d}, R. V. Skidanov^{b,d} and Payal Verma^b.

^aFísica i Cristal·lografia de Materials i Nanomaterials (FiCMA-FiCNA) and EMaS, Universitat Rovira i Virgili (URV), Marcel·lí Domingo 1, E-43007 Tarragona, Spain;

^bSamara State Aerospace University, 34 Moskovskoye shosse, Samara, Russia 443086;

^cDepartamento de Física de Materiales, Universidad Autónoma de Madrid, 28049 Madrid, Spain;

^dImage Processing Systems Institute of the Russian Academy of Sciences, 151 Molodogvardejskaya st., Samara, Russia 443001

ABSTRACT

In this work, we have demonstrated the use of different technologies to fabricate straight channel waveguides, S-bend waveguides, Y-splitter and Mach-Zehnder (MZ) structures on RbTiOPO₄ crystals and its isomorphs. We used reactive ion etching (RIE), inductively coupled plasma-RIE (ICP-RIE), femtosecond pulse laser micro-fabrication and ion diffusion techniques to structure these crystals. Computer simulations have been carried out and compared with the optical characterization of the waveguides which are in agreement with each other.

Keywords: RTP, Epitaxial layer, RIE, Ion exchange, femtosecond laser writing

1. INTRODUCTION

RbTiOPO₄ (hereafter RTP) belongs to the KTiOPO₄ (hereafter KTP) family of nonlinear optical crystals. RTP has orthorhombic symmetry, with $a=12.974(2)$ Å, $b=6.494(3)$ Å and $c=10.564(6)$ Å [1] with the space group $Pna2_1$. They are positive biaxial crystals, with $n_x < n_y < n_z$ (being the X, Y and Z dielectric axes parallel to crystallographic *a*, *b* and *c* directions, respectively). These crystals are known for their high electro-optical and nonlinear optical coefficients which make them attractive for electro-optic applications such as modulators and Q-switches [2]. These electro-optic properties of RTP crystals make them attractive for integrated optical applications for fabrication of active and passive devices.

1.1 Growth of the samples

RTP melts incongruently below its melting temperature at 1443 K [3, 4]. Therefore, under normal pressure, single crystals cannot be directly grown from the melt. Hydrothermal techniques [5] and high temperature solutions [6] have been successfully reported to grow these crystals. We grew RTP single crystals by using high temperature solution methods, using the top seeded solution growth slow cooling technique. All the growth experiments were performed in a vertical tubular single-zone furnace. The solution composition was chosen taking into account the RTP primary crystallization region in solutions with 20 mol% WO₃ [7]. The solution composition used was Rb₂O-P₂O₅-TiO₂-WO₃=44.24-18.96-16.8-20 (mol %). The solution was homogenized by maintaining the temperature at about 50-100 K above the expected saturation temperature for 3-5 h [7]. The saturation temperature of the solution was determined by observing the growth/dissolution of the seed in contact with the surface of solution. The supersaturation of the solution was obtained by applying slow cooling to the solution at a rate of 0.1 K/h for the first 15 K and then 0.05 K/h for the next 10-20 K. During the initial stage of growth, the crystal rotation was kept at 60 rpm and as the crystal was growing, the rotation was decreased progressively to 40 rpm in order to maintain the convection pattern. In several experiments, when the crystal dimension in the (001) plane was enough, a pulling rate of 1 mm per day was applied in order to increase the crystal dimension along the *c* direction. When the crystal was fully grown, it was slowly extracted from the solution and maintained slightly above the solution surface while the furnace was cooled at 30-40 K/h to room temperature. Finally, the substrates were obtained by cutting the bulk crystal perpendicular to the *c*- crystallographic direction and polishing it with diamond powder.

1.2 Epitaxial layer fabrication

The $\text{Rb}_{1-x-y}\text{TiYb}_x\text{Nb}_y\text{OPO}_4$ epitaxial layers were grown on RTP(001) substrates by Liquid Phase Epitaxial (LPE) method. The epitaxial growth was carried out in a vertical furnace with a wide zone where the temperature differences were practically zero. The solution composition used in these LPE experiments was $\text{Rb}_2\text{O}-\text{P}_2\text{O}_5-\text{TiO}_2-\text{Nb}_2\text{O}_5-\text{Yb}_2\text{O}_3-\text{WO}_3=43.9-23.6-20.7-0.45-1.35-10$ (mol %). In order to reduce the viscosity of the solution, WO_3 (10 mol %) has been introduced in the solution [7]. Careful determination of the saturation temperature of the solution was carried out by measuring the growth/dissolution rate of the crystal seed in contact with the surface of the solution while rotating at constant speed of 60 rpm. RTP substrates were first cleaned by using a mixture of $\text{HNO}_3/\text{H}_2\text{O}$ in the 50/50 ratio in volume for 5 min, followed by dipping in distilled water (5 min), then in acetone (5 min), and finally in ethanol (5 min). The entire cleaning process was carried out with the substrates rotating at 60 rpm. After that, the substrates were slowly introduced into the furnace using a stepper motor drive to avoid thermal shocks and maintain it for 1 h above the surface of solution to obtain thermal equilibrium between the solution and the substrate. Then the substrate was dipped into the solution at a temperature of 1 K above the saturation temperature for 5 min in order to dissolve the outer layer of the substrate. The epitaxial growth was carried out on the RTP substrate at a temperature 3 K below the saturation temperature for 3 h, with the substrate rotating at 60 rpm. After the epitaxial growth process, the sample was extracted slowly from the solution and held a few mm above the solution, while the furnace was cooled down to room temperature at a rate of 25 K/h, to avoid thermal shock. After that, a cladding layer of undoped (RTP) was grown by LPE method as mentioned above. Finally, the cladding layer was polished in order to obtain a smooth surface for the deposition of metal mask to be used in ICP-RIE for the microstructuring of the cladding layer. The as-grown RTP single crystal and (Yb,Nb):RTP epitaxial layer grown on polished substrate were shown in figure 1.

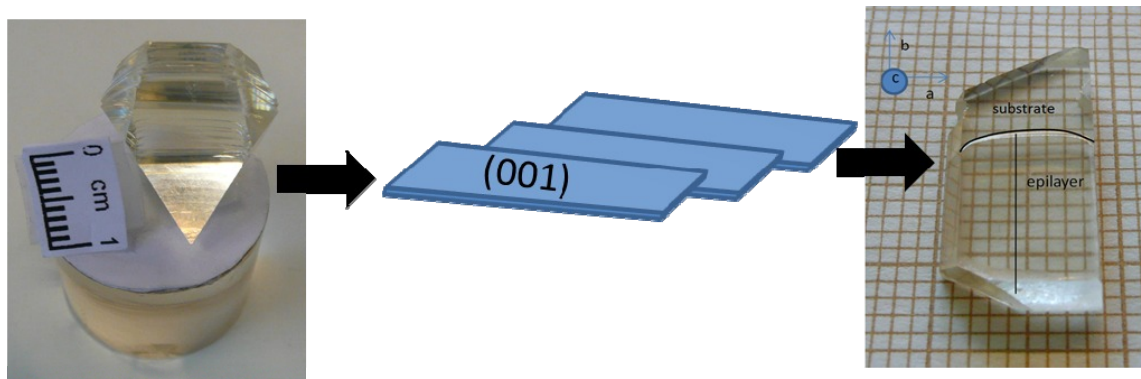


Figure 1. As grown RTP single crystal, scheme of the cutting process and as grown epitaxy.

2. FABRICATION TECHNIQUES

2.1 Fabrication of Y-splitters and Mach-Zehnder Structures on (Yb,Nb):RTP/RTP epitaxial layers by Reactive Ion Etching

The reactive ion etching structuring of the RTP (001) substrates and (Yb,Nb):RTP/RTP (001) epitaxial layers has been performed using fluorine chemistry. Liquid phase epitaxial growth of cladding layers has also been performed, resulting in a high-quality interface growth without appreciable defects. 9-mm long Mach-Zehnder and Y-splitter structures were designed and patterned in RTP substrates and in (Yb, Nb):RTP/RTP(001) epitaxial layers. A maximum etch rate of 8.7 nm/min was obtained (gases used Ar, SF_6), and the deepest etch achieved was 3.5 μm . The refractive index difference between the (Yb, Nb):RTP layer and the RTP substrate at 1.5 μm has been measured and optical waveguiding at this wavelength has been demonstrated [8].

In order to characterize the propagation modes of MZ, the sample was polished perpendicular to *a* crystallographic direction (X axis), and the light will propagate in this direction. The near field pattern was measured using an IR camera in order to visualize the mode intensity profile at the output of a MZ. Figure 2 (a) shows the near field pattern of the output TM mode guided in a MZ. Figure 2 (b) shows the output TM mode obtained by the simulation. The horizontal and vertical fundamental TM mode field diameters (MFD) at $1/e^2$ intensity (shown in figure 2 (c) and 2 (d), respectively)

were measured to be 17.6 μm and 8.3 μm , along the b (horizontal) and c (vertical) directions, respectively. The dimensions of the simulated guided mode are 23.3 μm and 9.6 μm along b (horizontal) and c direction (vertical) respectively, and the refractive index contrast for n_z at 1,5 microns is 0.005.

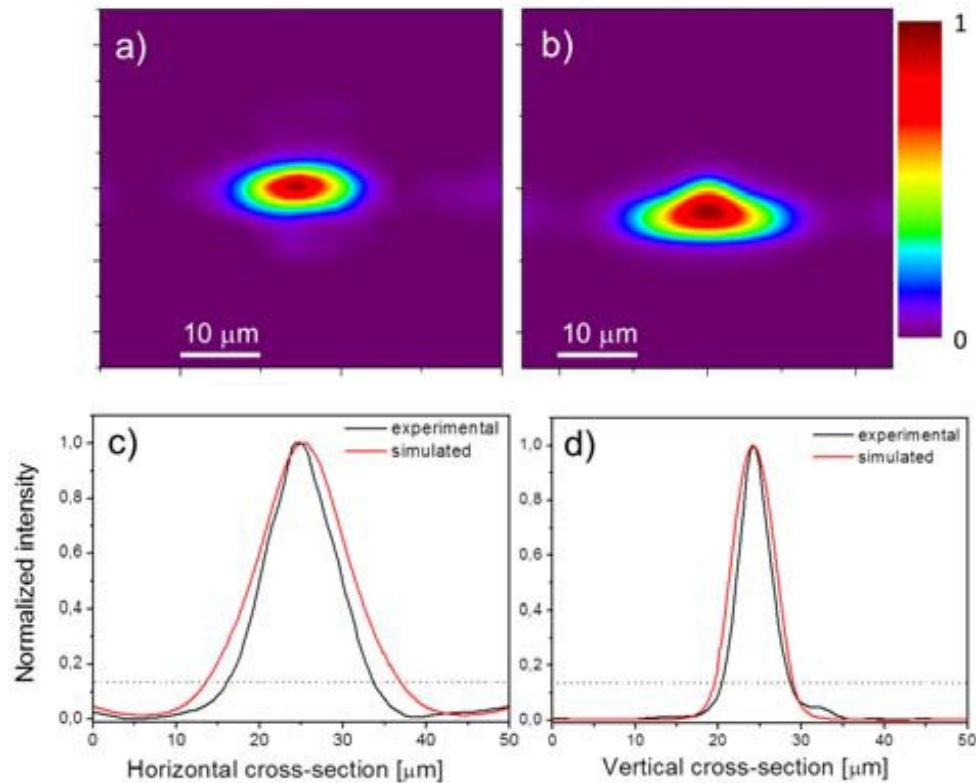


Figure 2. (a) Near- field TM mode image of the MZ waveguide (b) Simulated TM mode of the MZ waveguide (c) Horizontal cross-section of the experimental and simulated TM guided mode, (d) Vertical cross-section of the experimental and simulation TM mode.

The optical characterization of 9 mm long Y-splitter is shown in figure 3 (a). The simulation of the modes is plotted in Figure 3(b). The Y-splitter is rather well balanced, obtaining an output flux power ratio between the two branches of 0.91. The horizontal and vertical fundamental MFD at $1/e^2$ intensity (shown in Figure 3(c) and 3(d), respectively) were measured to be 19 μm and 16.7 μm (right and left branches, respectively) along the b direction and 9.6 μm and 9.9 μm (right and left branches, respectively) along the c direction. The MFD for the simulated modes were 8.4 μm and 17.6 μm , for the vertical and horizontal directions, respectively. The separation between the centers of two modes emitting from two respective arms is around 36 μm .

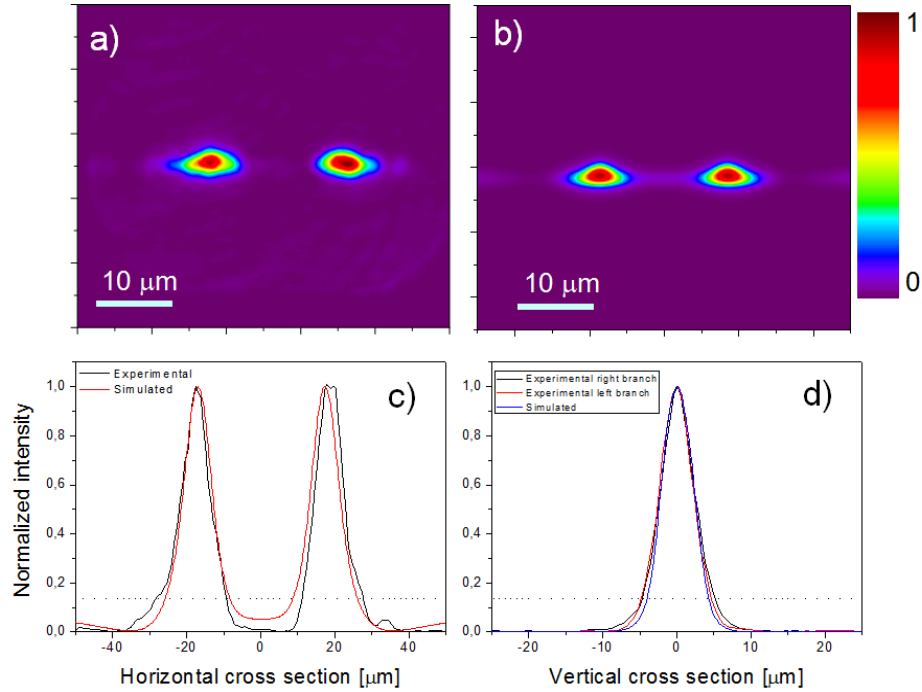


Figure 3. (a) Near- field TM mode image of a waveguide Y-splitter, (b) Simulated TM mode of the Y-splitter waveguide, (c) Horizontal cross-section of the experimental and simulated guided TM modes, (d) Vertical cross-section of the experimental and simulation TM modes.

2.2 Channel waveguides fabrication technique in RbTiOPO_4 planar waveguides by structuring the cladding layer with Induced Coupled Plasma-Reactive Ion etching (ICP-RIE)

ICP-RIE has been used to produce ridge waveguides in RTP crystals. A thin layer of a RTP planar waveguide doped with Yb and Nb was grown on a RTP substrate with an additional RTP cladding layer grown by LPE method. Then the cladding layer was structured by ICP-RIE in such a way that lateral confinement of the light was achieved by a local increase of the effective refractive index of the planar waveguide. ICP-RIE etching on RTP (001) surface has been done by using Argon and SF_6 gas (ratio between gases 50:50), achieving an etch rate of around 150 nm/min with very low roughness (around 4 nm). The dimensions of the straight waveguides were optimized by simulation with Rsoft beamPro software based on light propagation method to obtain guiding with a single optical mode at 1.5 μm.

In Figure 4, we can observe ESEM images of the channels fabricated by ICP-RIE in a RTP cladding, using a Ti-Cr mask with designed structures of 30 μm in width. Figure 4 (a) shows the cross-sectional view of the sample with epitaxial and cladding layer prior to etching. The etching time was 45 min and the etch depth obtained was around 5.7 μm. Ribs with trapezoidal cross section were obtained in the cladding layer as shown in figure 4 (b). There are no appreciable defects at the interfaces between the RTP substrate-epitaxial layer and the epitaxial layer-cladding layer. The bottom of the channels is found to be approximately 31 μm in width, while at the top the channels width is around 25 μm.

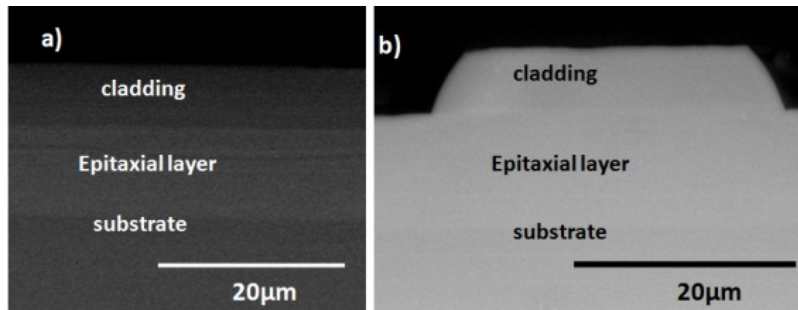


Figure 4. (a) ESEM image of the sample before etching process, (b) cross-sectional image of the proposed waveguides.

The vertically polarized 1520 nm light of a HeNe laser with a maximum output power of 1 mW was coupled to 9 mm long stripe loaded waveguides. The near field pattern was measured using an IR camera in order to visualize the mode intensity profile at the output of the stripe loaded waveguide; Figure 5 (a) shows the near-field pattern of an output mode guided in a channel. The horizontal and vertical fundamental mode field diameters (MFD) at $1/e^2$ intensity (shown in figure 5 (c) and figure 5(d) were measured to be 26.5 μm and 20.7 μm , along the b (horizontal) and c (vertical) directions, respectively. Figure 5 (b) shows the mode profile of the simulated data with a horizontal and vertical dimension of 24.7 μm and 12.3 μm respectively. The horizontal fundamental mode field diameter obtained by simulation show an agreement with the experimental results but in case of vertical field diameter it has a contradiction that could be due to the big size of coupling mode used in the experiment.

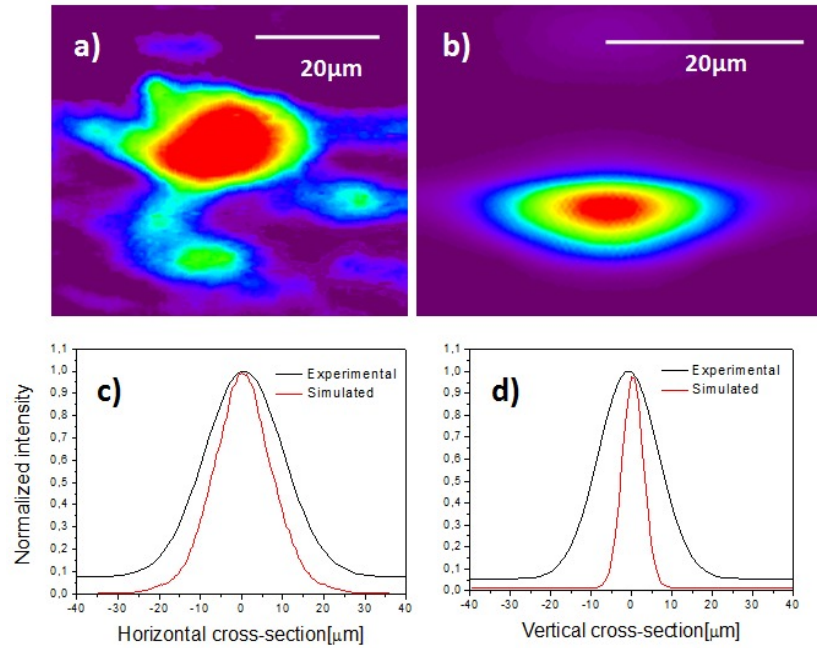


Figure 5. (a) Near- field pattern of an experimental guided mode, (b) simulated mode, (c) horizontal cross-section of the experimental and simulated guided modes, (d) vertical cross-section of the experimental and simulated guided modes.

2.3 Low-repetition rate femtosecond laser writing of optical waveguides in KTP crystals: analysis of anisotropic refractive index changes

We have reported the direct low-repetition rate femtosecond pulse laser microfabrication of optical waveguides in KTP crystals and the characterization of refractive index changes after the thermal annealing of the sample, with the focus on studying the potential for direct laser fabricating MZ optical modulators. We have fabricated square cladding waveguides by means of stacking damage tracks, and found that the refractive index decrease is large for vertically polarized light (c -axis; TM polarized) but rather weak for horizontally polarized light (a -axis; TE polarized), this leading to good near-infrared light confinement for TM modes but poor for TE modes. However, after performing a sample thermal annealing we have found that the thermal process enables a refractive index increment of around 1.5×10^{-3} for TE polarized light, while maintaining the negative index change of around -1×10^{-2} for TM polarized light.

In order to evaluate the local refractive index changes we have followed a multistep procedure: We have first characterized the waveguide cross-sections by means of Raman micro-mapping to access the lattice micro-modifications and their spatial extent. Secondly we have modeled the waveguides following the modified region sizes obtained by micro-Raman with finite element method software to obtain a best match between the experimental propagation modes and the simulated ones. Furthermore we also report the fabrication of MZ structures and the evaluation of propagation losses [9].

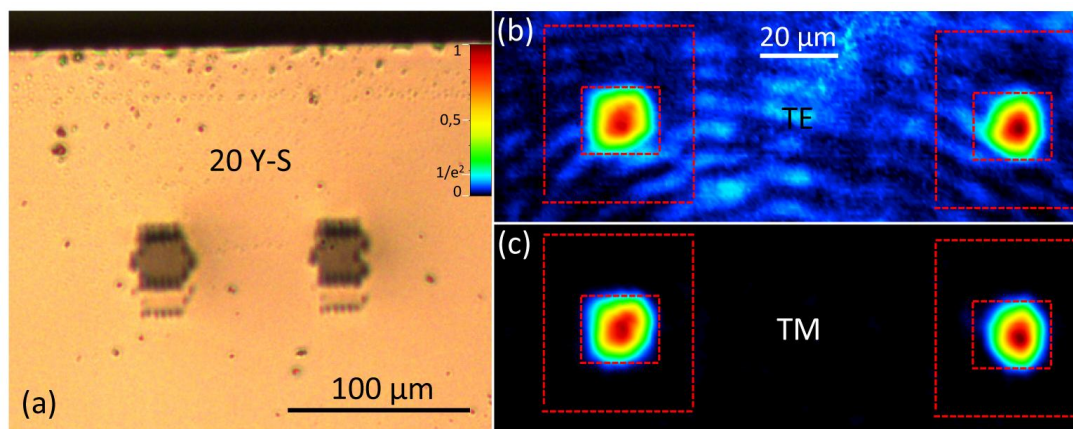


Figure 6. Microscope pictures (a) and output fundamental modes of Y-splitter for both TE (b) and TM polarizations (c).

In order to evaluate how the cladding waveguide split the modes in two, Y-splitters were also characterized in its output. Figure 6 (a) shows the recorded micrographs, as well as the fundamental modes obtained by careful alignment of the input beam relative position to the straight waveguide inputs. As it can be observed in Figure 6, the as fabricated waveguide structures do not confine TE light inside the cladding, whereas for TM polarized light the confinement is rather good as observed in Figure 6 (c). Note that higher order modes were also observed, but are not shown here for the sake of brevity. As previously mentioned, to obtain a purely single mode behavior the 20 μm width claddings should be reduced to around half the width so that no higher orders could be supported.

2.4 Channel waveguides and Mach-Zehnder structures on RTP by Cs⁺ ion exchange

Cs⁺ ion diffusion in RTP and (Yb,Nb):RTP/RTP (001) has been used to increase the refractive indices for preparing waveguides with designed patterns. Ti masks were fabricated on the RTP samples by conventional photolithography. Cs⁺ diffusion was done using CsNO₃ melt at 698 K during 2 h. Elemental analysis confirms a Cs⁺ exponential profile, with a variable depth. Apparently the Cs⁺ diffusion is disfavored in the doped epitaxial sample. The refractive index contrast is higher in n_z than in $n_{x,y}$. Near field images of the guided modes at 632, 1064 and 1520 nm were recorded [10].

Figure 7 shows the Cs⁺ concentration as a function of the distance from the crystal surface in three different channels in the RTP and two other channels in a (Yb,Nb):RTP epitaxial layer. As can be observed there's no reproducibility of the exchange in the different channels, which may be due to each channel being located in a different crystal growth sector, and then, different ferroelectric domains. It can be also observed that the quantity of Cs⁺ introduced in RTP is larger than in the doped (Yb,Nb):RTP. This may be expected due to the similar or lower ionic conductivity when RTP is doped with Yb and Nb [11]. In Gavalda *et al.* [11], the Nb content of the sample was larger than in the epitaxial sample reported in this work, and the ytterbium concentration was similar; and it was observed that the couple (Yb,Nb) has similar ionic conductivity than RTP along c , but when compared with single doped Nb samples, the codoping (Yb,Nb) decreases the ionic conductivity along c , so the tendency observed in our samples, is in agreement with the reported tendency of the ionic conductivity. Generally, the Cs⁺ concentration decreases with depth and the exchange region is as minimum 6-7 μm.

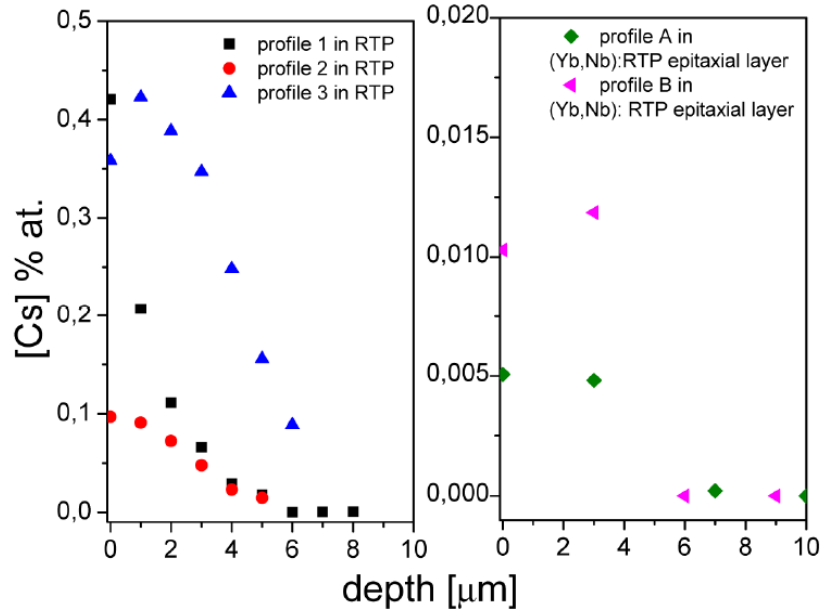


Figure 7. Cs⁺ concentration in the channel as a function of the depth in the RTP substrate and (Yb,Nb):RTP epitaxial layer.

Y-splitters of 9 mm length were characterized at 1520 nm light in TM polarization. A Gaussian profile of Y-splitter with dimensions of 15.6 μm x 9.0 μm for the left arm and 13.2 μm x 8.5 μm for the right arm of Y-splitter in the *b* and *c* direction respectively was measured as shown in figure 8.

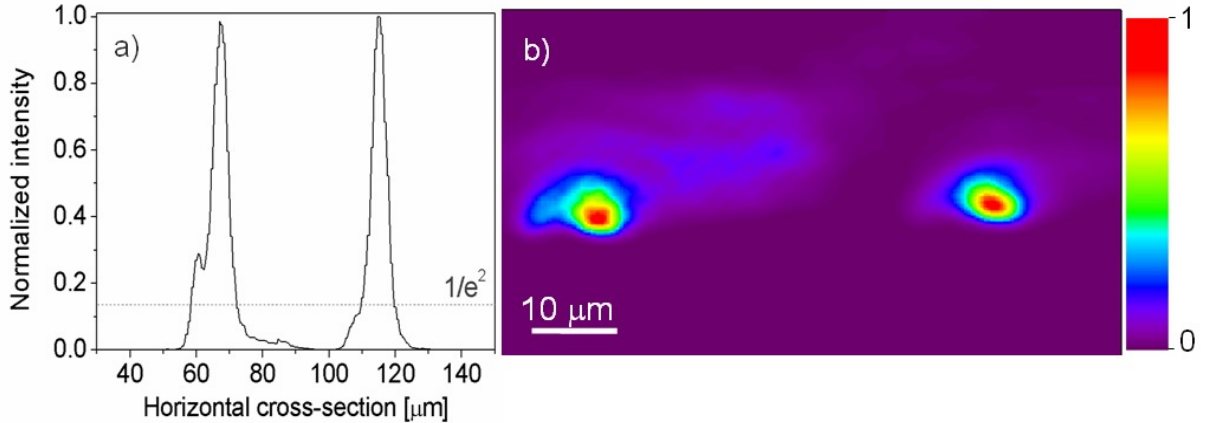


Figure 8. (a) Horizontal cross-section of the experimental guided TM modes, (b) Near-field pattern of an experimental guided mode.

CONCLUSIONS

This paper presented the use of different technologies to fabricate straight channel waveguides, S-bend waveguides, Y-splitter and Mach-Zehnder structures on RbTiOPO₄ crystals and its isomorphs. These crystals are known for their high electro-optical and nonlinear optical coefficients which make them attractive for electro-optic applications such as modulators and Q-switches. These electro-optic properties of RTP crystals make them attractive for integrated optical applications for fabrication of active and passive devices.

ACKNOWLEDGEMENTS

This work is supported by the Ministry of Education and Science of the Russian Federation, Russian Science Foundation (grant No. 14-19-00114), Spanish Government under Projects MAT2011-29255-C02-02, TEC2014-55948-R, MAT2013-47395, C4-4-R/1-R and by the Catalan Authority under Project 2014SGR1358.

REFERENCES

- [1] Thomas, P. A., Mayo, S. C., and Watts, B. E., "Crystal structures of RbTiOAsO_4 , $\text{KTiO}(\text{P}_{0.58}\text{As}_{0.42})\text{O}_4$, RbTiOPO_4 and $(\text{Rb}_{0.465}\text{K}_{0.535})\text{TiOPO}_4$, and analysis of pseudosymmetry in crystals of the KTiOPO_4 family," *Acta Cryst. B*, 48, 401-407 (1992).
- [2] Satyanarayan, M.N., Deepthy, A., and Bhat, H. L., "Potassium titanyl phosphate and its isomorphs: growth, properties, and applications," *Crit. Rev. Solid State Mater. Sci.*, 24(2), 103-191 (1999).
- [3] Cheng, L. K., Bierlein, J. D., "Crystal growth of KTiOPO_4 isomorphs from tungstate and molybdate fluxes," *J. Cryst. Growth* 110(4), 697-703 (1991).
- [4] Voronkova, V. I., Yanovskii, V. K., "Flux growth and properties of the KTiOPO_4 family crystals," *Neorg. Mater.* 24(2), 273-277 (1988).
- [5] Laudise, R. A., Sunder, W. A., "Solubility and P-V-T relations and the growth of potassium titanyl phosphate," *J. Cryst. Growth* 102(3), 427-433 (1990).
- [6] Bordui, P. F., Jacoo, J. C., Loiacono, G. M., Stolzenberger, R. A., Zola, J. J., "Growth of large single crystals of KTiOPO_4 (KTP) from high temperature solution using heat pipe based furnace system," *J. Cryst. Growth* 84(3), 403-408 (1987).
- [7] Carvajal, J. J., Nikolov, V., Solé, R., Gavalda, J., Massons, J., Rico, M., Zaldo, C., Aguiló, M., Díaz, F., "Enhancement of the erbium concentration in RbTiOPO_4 by codoping with niobium," *Chem. Mater.* 12(10), 3171-3180 (2000).
- [8] Butt, M. A., Solé, R., Pujol, M. C., Ródenas, A., Lifante, G., Choudary, A., Murugan, G. S., Shepherd, D. P., Wilkinson, J. S., Aguiló, M., and Díaz, F., "Fabrication of Y-splitters and Mach-Zehnder Structures on (Yb, Nb): RbTiOPO_4 / RbTiOPO_4 Epitaxial Layers by Reactive Ion Etching," *J. Lightwave Technol.* 33(9), 1863-1871 (2015).
- [9] Butt, M. A., Nguyen, H. D., Ródenas, A., Romero, C., Moreno, P., Aldana, J. R.V., Aguiló, M., Solé, R. M., Pujol, M. C., and Díaz, F., "Low-repetition rate femtosecond laser writing of optical waveguides in KTP crystals: analysis of anisotropic refractive index changes," *Opt. Express*, 23(12), 15343-15355 (2015).
- [10] Butt, M. A., Pujol, M. C., Solé, R., Ródenas, A., G. Lifante, G., J.S. Wilkinson, J. S., Aguiló, M., and Díaz, F., "Channel waveguides and Mach-Zehnder structures on RbTiOPO_4 by Cs^+ ion exchange," *Opt. Mater. Express*, 5(5), 1183-1194 (2015).
- [11] Gavalda, J., Carvajal, J. J., Mateos, X., Aguiló, M., and Díaz, F., "Dielectric properties of Yb^{3+} and Nb^{5+} doped RbTiOPO_4 single crystals," *J. Appl. Phys.* 111(3), 034106 (2012).